Volume 15
Number 1
January 2022
Pages 1–400

Energy & Environmental Science

rsc.li/ees

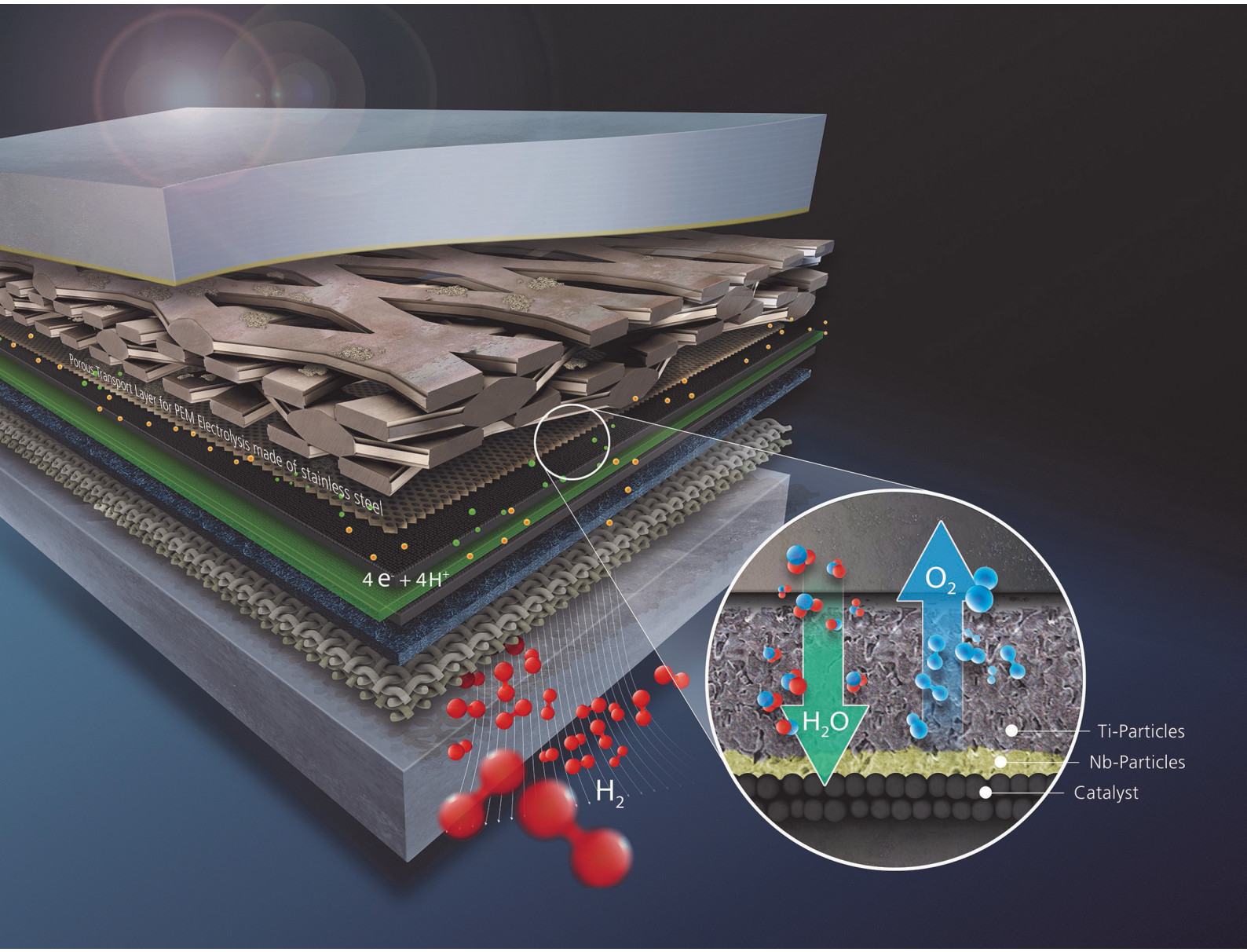

ISSN 1754-5706

ROYAL SOCIETY OF CHEMISTRY

PAPER
A. S. Gago *et al.*
A high-performance, durable and low-cost proton exchange membrane electrolyser with stainless steel components

Energy & Environmental Science

ROYAL SOCIETY OF CHEMISTRY

PAPER

View Article Online
View Journal | View Issue

Cite this: *Energy Environ. Sci.*, 2022, **15**, 109

A high-performance, durable and low-cost proton exchange membrane electrolyser with stainless steel components†

S. Stiber, [a] N. Sata, [a] T. Morawietz,[a] S. A. Ansar,[a] T. Jahnke,[b] J. K. Lee,[c] A. Bazylak, [c] A. Fallisch,[d] A. S. Gago *[a] and K. A. Friedrich [ae]

Proton exchange membrane water electrolysis (PEMWE) is the most promising technology for sustainable hydrogen production. However, it has been too expensive to compete with current state-of-the-art technologies due to the high cost of titanium bipolar plates (BPPs) and porous transport layers (PTLs). Here, we report a high-performance, durable and low-cost PEMWE cell with coated stainless steel (ss) BPPs and PTLs. When using uncoated ss components in the PEMWE cell, the cell depolarizes rapidly, reaching 2 V at only 0.15 A cm^{-2}. After the application of non-precious metal coatings of Ti and Nb/Ti on the ss-BPP and ss-PTL, respectively, the current density can be increased by a factor of 13 while maintaining the same performance. Extensive physical and electrochemical characterization supported by pore network modelling shows that the Nb/Ti coating on the ss-PTL leads to efficient water and gas transport at the interface with the anode. The PEMWE cell with coated ss components was evaluated in an accelerated stress test (AST) for more than 1000 h. No sign of Fe contamination in either the membrane or the electrodes is observed at the end of the test. With our results, we demonstrate that PEMWE cells can be manufactured almost entirely in ss, facilitating an unprecedented cost reduction in this technology and advancing the widespread use of green H_2.

Received 8th July 2021,
Accepted 22nd September 2021

DOI: 10.1039/d1ee02112e

rsc.li/ees

Broader context

Global warming due to high CO_2 emissions worldwide is one of the greatest challenges of the 20th century. In the last few years, it has become clear that the current political agreements and efforts will probably not contribute to a sufficient reduction of CO_2 emissions. Besides energy and heat generation, the chemical industry and the mobility sector are some of the largest emitters of CO_2. Alternatives to the use of fossil fuels must be found for the respective sectors and integrated into the processes in order to stop the steady upward trend. It is therefore essential to tighten up the already ambitious targets set out in the Paris Agreement and to push ahead the expansion of renewable energies. However, energy supply based on renewable energies entails dependence on weather conditions and geographical locations. Both, wind and sun, are not necessarily available when and where energy is needed. Here, hydrogen production *via* water electrolysis using renewable electricity (green hydrogen) can decouple energy production from actual demand in terms of time, and energy can thus be stored. Proton exchange membrane water electrolysis (PEMWE) is the most suitable technology for this purpose but is still expensive and mainly due to the use of titanium for manufacturing stack components such as bipolar plates (BPP) and porous transport layers (PTLs). Herein, we report a PEMWE cell that is almost fully made of stainless steel, exhibiting high performance and durability. As BPPs and PTLs are made of titanium, the most expensive components of the electrolyzer stack, a significant cost reduction in this technology has been achieved by showing that they can be manufactured in stainless steel. This PEMWE cell with stainless steel components will contribute to the widespread production of green hydrogen.

[a] *Institute of Engineering Thermodynamics/Electrochemical Energy Technology, German Aerospace Center (DLR), Pfaffenwaldring 38-40, 70569 Stuttgart, Germany. E-mail: aldo.gago@dlr.de; Fax: +49 711 6862-747; Tel: +49 711 6862-8090*

[b] *Institute of Engineering Thermodynamics/Computational Electrochemistry, German Aerospace Center (DLR), Pfaffenwaldring 38-40, 70569 Stuttgart, Germany*

[c] *Department of Mechanical and Industrial Engineering, Faculty of Applied Science and Engineering, University of Toronto Institute for Sustainable Energy, University of Toronto, Toronto, Ontario, M5S 3G8, Canada*

[d] *Fraunhofer-Institut für Solare Energiesysteme ISE, Heidenhofstraße 2, 79110 Freiburg, Germany*

[e] *Institute of Building Energetics, Thermal Engineering and Energy Storage (IGTE), University of Stuttgart, Pfaffenwaldring 31, 70569 Stuttgart, Germany*

† Electronic supplementary information (ESI) available. See DOI: 10.1039/d1ee02112e

1. Introduction

Currently, the main commercial electrolytic technologies for the large-scale production of hydrogen are alkaline water electrolysis (AWE) and proton exchange membrane water electrolysis (PEMWE).[1] AWE is already a well-developed technology, but issues in terms of gas purity, safety and response time remain.[2] PEMWE, on the other hand, is a promising candidate that exhibits high efficiency, a rapid response and a wide dynamic operation range within an easy-to-maintain compact design and a simple auxiliary system.[3] The main drawback of

PEMWE compared with that of alkaline water electrolysis is the high capital cost: €600 kW^{-1} alkaline *vs.* €900 kW^{-1} PEMWE.[4]

The main components of a PEMWE cell are the catalyst coated membrane (CCM), porous transport layers (PTLs) and bipolar plates (BPPs). The CCM consists of iridium and ruthenium oxides (IrO_x–RuO_y) as the anode and platinum nanoparticles supported on carbon (Pt/C) as the cathode. Besides the BPPs, the PTL is one of the key components of a PEMWE cell that allows effective transport of reactant water to the electrodes while facilitating gas removal towards the flow field of the BPP. Efficient gas/water management has a high impact on the cell performance due to the reduction in mass transport losses.[5–7] On the cathode side, carbon paper is a state-of-the-art PTL material, which is often used in PEM fuel cells (FC).[8] On the anode side, titanium is widely used for PTLs since titanium can withstand the harsh conditions of a highly concentrated O_2 environment and elevated cell potentials (>2 V).[3] Commercially available PTLs for the anode include sintered powders, felts, and meshes sold by companies such as GKN Sinter Metals, Bekaert and Melicon, respectively. Recent developments have included tunable PTLs with controlled porosities[9,10] and pore structures with a size gradient.[11,12]

Manufacturing sophisticated porous structures such as sintered powders or felts in titanium is cost prohibitive. Moreover, to avoid passivation, which leads to an increase in cell voltage over time,[13,14] titanium must be coated with platinum group metals (PGMs). A stainless steel PTL (ss-PTL) would be preferable, but it severely corrodes, thus poisoning the CCM with Fe and Ni.[15,16] Our previous developments have demonstrated that it is possible to use ss as a base material for manufacturing the BPP. A dense coating applied by plasma spraying provides full protection against corrosion in the aggressive PEMWE environment.[17] These coatings have been integrated into commercial electrolyser stacks and tested for more than 1000 h without the ss substrate showing any signs of corrosion.[18,19] Likewise, physical vapor deposition (PVD) applied Ti/TiN coatings on steel components could be considered for anode-side application in PEMWE cells, which have already been evaluated for their suitability by N. Rojas *et al.*[20] However, a test in a real PEMWE cell was not carried out here. Complementing the anode-side use of the Nb/Ti coated steel BPP, Shirvanvian P. *et al.* see laser-treated 316L stainless steel, carbon-based and nitride coatings on stainless steel, as already investigated for the PEMFC cell, as possible components for cathode-side use as the BPP in PEMWE cells.[21]

Depending on the cell configuration, *e.g.*, with or without a flow field in the BPP, the PTL and the BPP together approximately represent between 70%[22] and 60%[23] of the PEMWE stack cost. The cost of Ir catalyst is the other key cost driver in PEMWE systems and it will become increasingly important as the large-scale manufacturing cost of PTLs and BPPs is reduced. There have been some attempts to use ss-PTLs in PEMWE cells. J. Mo *et al.* tested an uncoated mesh type ss-PTL in a PEMWE cell.[16] The ss-PTL corroded rapidly and the realised Fe poisoned heavily the CCM. Another attempt was made by N. F. Daudt *et al.* in which they sintered a Nb coating on a ss-PTL.[24] From their PEMWE tests, one can notice that the slopes of their polarization curves with the coated ss-PTL bend sharply upwards at *ca.* 1 A cm^{-2}, which is an indication of either mass transport losses or severe degradation. The authors do not report any stability test though.

A complete PEMWE stack manufactured mainly in ss, that is, PTLs and BPPs, remains an important challenge. Such a stack could drastically reduce the PEMWE cost for large-scale applications, making green hydrogen more competitive. In this work, we report the first efficient, stable and high performance PTL made of ss coated with non-precious Nb/Ti metal by plasma spraying. The coating not only protects the PTL against corrosion but also significantly improves the cell performance. Through extensive characterization and numeric simulation, we provide a comprehensive explanation of this improved performance. The coated ss-PTLs in combination with our previous development of coated ss-BPPs allow the production of a PEMWE cell with all metallic components made of ss, thus marking an unprecedented cost reduction in this technology.

2. Methods

2.1. Plasma-sprayed coatings

Coatings of Nb/Ti were produced by vacuum plasma spraying (VPS) on 4-layer mesh-type ss PTLs (GDL MeliDiff in 1.4404, Melicon GmbH). The chamber pressure was 40 mbar. The coating powders were grade 1 Ti (TLS Technik Spezialpulver) and Nb (H.C. Starck, currently FST Flame Spray Technologies) with a particle size of <45 μm. The gas flow rates of Ar, N_2 and H_2 were carefully controlled to achieve the needed plasma enthalpy of 12.5 MJ kg^{-1} for the Ti and Nb layers. Six coating runs with Ti were first applied; specifically, the plasma spray gun was oscillated over the substrates six times during the coating process. Subsequently, two additional coating runs of Nb were sprayed on top of the finest mesh of the multi-layer mesh-type PTL. The torch sweep rates were 600 mm s^{-1} for all the samples. Before deposition, the PTL substrates were heated to 250 °C. The produced PTL is labelled Nb/Ti/ss-PTL. In Fig. 1 the ss-PTL sample with the Nb/Ti coating is shown schematically. For comparison purposes, similar coatings were applied on 4-layer mesh-type Ti-PTLs (GDL MeliDiff in Ti Grade 1, Melicon GmbH). The resulting sample is labelled Nb/Ti/Ti-PTL.

2.2. Physical characterization

2.2.1. Scanning electron microscopy (SEM). SEM was used to analyse the morphology of the produced coated samples. For all samples, cross-sectional images were recorded with an FE-SEM Zeiss ULTRA plus in secondary electron mode with charge compensation. The working distance and accelerating potential were between 8.0 and 8.3 mm and 20 kV, respectively. The purity of the Nb/Ti coatings was determined by energy-dispersive X-ray spectroscopy (EDS) using an annular back-scatter detector (AsB) for high material contrast. For the elemental mapping on post-tested CCMs, a JEOL JSM7200F equipped with a Bruker Quantax energy-dispersive X-ray system was used. The working distance was between 10.2 and

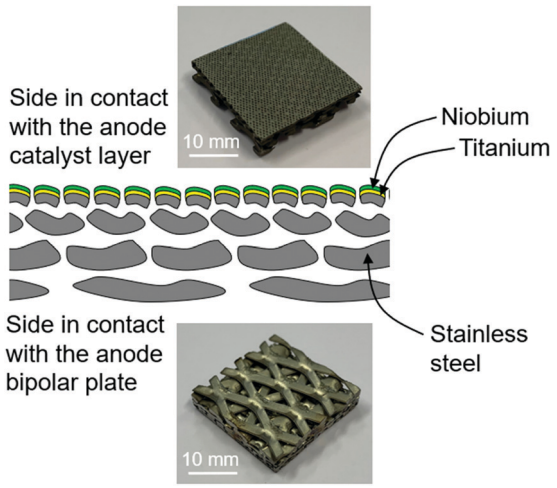

Fig. 1 Scheme of the ss-mesh PTL with a plasma-sprayed Nb/Ti coating at the interface with the anode catalyst layer.

12.5 mm, while the accelerating potential was reduced to 15 kV. The mapping was performed with 2 μm per pixel and a pixel time of 128 μs for 10 cycles. The images were averaged with Esprit 2 software for noise reduction.

2.2.2. Mercury intrusion porosimetry (MIP) and X-ray computed tomography (CT). The porosities of the Nb/Ti coatings on ss-PTL and Ti-PTL were determined by MIP up to a pressure of 200 MPa (Pascal 140/240, Thermo Scientific). Prior to the measurements, the samples ($\sim 1 \times 2$ cm^2) were dried in an oven at 60 °C overnight. Since the MIP of the coated samples was performed on the top mesh of the PTL substrates, the obtained pore volume was the overall sum in both the finest mesh of the substrate and the coating. The geometrical parameters of the samples were taken into consideration, and their mathematical formulation is provided in eqn (1), with which the coating porosity can be estimated:

$$p_{\mathrm{coat}} = \frac{1}{\left(1 + \dfrac{m_{\mathrm{coat}} \times 1000}{\delta_{\mathrm{theoretical}} \times V^{\mathrm{p}}_{\mathrm{coat}} \times m_{\mathrm{sample}}}\right)} \quad (1)$$

here, p_{coat}, $V^{\mathrm{p}}_{\mathrm{coat}}$ [mm^3 g^{-1}], m_{sample} [g], m_{coat} [g] and $\delta_{\mathrm{theoretical}}$ [g cm^{-3}] are the coating porosity, pore volume of the coating per total sample weight, total sample weight, weight of the coating and theoretical density of the coating, respectively. Classically, the quotient of the pore volume of the sample given by the MIP and the sample volume is used. However, for samples made of a relatively thick substrate and thin coating, this calculation becomes inaccurate. Therefore, $V^{\mathrm{p}}_{\mathrm{coat}}$ is calculated based on data from two measurements by subtracting the pore volume of the uncoated mesh, which was determined by MIP, from the total pore volume of the sample, *i.e.*, the substrate and coating. m_{coat} is calculated using the weight ratios of the mesh before and after coating.

X-ray CT analysis was performed with a multi-scale X-ray nanotomograph (Skyscan 2211, Bruker). The reconstructed sample volume was 484.4 × 1386 × 1649.9 μm^3, achieving a resolution of 0.7 μm. An acceleration potential of 70 kV was used.

2.2.3. Interfacial contact resistance. The effect of the Nb/Ti coating on the interfacial contact resistance (ICR) of the ss-PTLs with respect to the compaction force was measured based on the method previously reported for measuring the coated BPP.[19] First, all PTL samples were cleaned before being measured by immersing them in deionized (DI) water and isopropanol baths and applying ultrasonication for 10 minutes after each step. The last cleaning cycle was carried out with DI water for 5 minutes, and thereafter, the PTL samples were placed in an oven for 20 minutes at 60 °C. Second, ICR measurements were performed by sandwiching the cleaned PTLs with a titanium plate (3.7025) and a TGP-H-90 between two gold-coated copper cylinders (inset of Fig. 5). The experimental setup was set in a hydraulic press, and a weight of 20 to 200 kg was applied in steps of 20 kg. The cylinders were connected to a potentiostat/galvanostat (Zahner Elektrik IM6) with a booster (Module PP240). A constant current of 1.25 A cm^{-2} was applied, and the response voltage was monitored. The ICR between the carbon paper and the Nb/Ti coating was determined by $R_{\mathrm{C/Coating}} = R_{\mathrm{measured}} - R_{\mathrm{C/Au}}$, where $R_{\mathrm{C/Au}}$ is the ICR of the carbon paper with the Au-coated cylinder. The Nb/Ti/Ti-PTL, uncoated Ti-PTL and ss-PTL were also measured for comparison purposes.

2.3. Pore network modelling

Pore network modelling (PNM) was conducted to elucidate the microscale mass transport behaviour on the Nb/Ti coating. Due to the vastly different length scales in the mesh pores, only the finest mesh layer and the Nb/Ti coating were considered as the simulation domain. Based on the CT images, a binarized 3D reconstruction was created using GeoDict®.[25] The resolution was 0.7 microns per pixel, and the domain was cropped to 1250 × 1250 × 230 pixels. The pore network was extracted from the binarized CT images using the marker-based watershed segmentation algorithm developed by Gostick *et al.*[26] In the pore network simulations, the pores of the network were represented with spheres connected by cylindrical throats, while the spatial distribution of the pores and the total void space were kept intact. The simulation was performed using an open source PNM package, OpenPNM.[27] The drainage of a wetting phase (liquid water) due to the invasion of a non-wetting phase (oxygen gas) was simulated on the coating network. In this drainage process, all throats connected to the inlet surface satisfying the entry (threshold) capillary pressure were invaded. The entry threshold capillary pressure of the cylindrical throats was approximated using the Young–Laplace equation:

$$P_{\mathrm{c}} = \frac{2\gamma \cos\theta}{r} \quad (2)$$

where γ is the surface tension [N m^{-1}], θ is the contact angle [radians], and r is the radius of the throat [m].

2.4. PEMWE tests

Conventionally, PEMWE cell components are tested in a setup such as that shown in Fig. 2a. In this system, fresh DI water is

continuously pumped through the PEMWE cell, entering separately on each electrode side through the inlets. It flows through the PTLs to the active site of the catalyst layers and then exits the cell through the outlets. Subsequently, the water and the product gases are driven to the anode and cathode water loops that make up the balance of the plant and include many components, such as ss pipes, pumps, gas separators, water conductivity sensors, ion exchange resins, and electro-mechanical valves. In this setup, cell degradation due to the poisoning of the CCM by the transport of metal ions can require thousands of hours of operation.[28,29] Most of the corrosion products from the cell will redeposit on the metallic parts that comprise the balance of plant (BoP), and only after long-term periods will they appear on the electrodes and membrane. Therefore, an accelerated stress test (AST) is required to evaluate the potential of a novel high-risk component, such as a coated ss-PTL, for implementation in commercial PEMWE.[30]

In contrast, such as the setup in Fig. 2b, the anode and cathode water loops of the BoP are kept as simple as possible. There are no ss pipes, pumps or any other metal parts in which ions could redeposit. The inlets and outlets of the cell are connected to small volume water reservoirs that are opened to the air. The water is fed to the cell *via* natural flow and the water level is kept constant by filling periodically with fresh water. This setup does not contain an ion exchange resin. Therefore, in this setup, any Fe^{2+} released due to the corrosion of Nb/Ti/ss-PTLs will rapidly poison the CCM as the water volume is kept small and constant. Any other impurities in the DI water, such as Ca^{2+}, Cu^{2+}, Na^{1+}, organics and metal ions in the ppm range, also continuously increase with each refill. Consequently, the cells with either Ti-PTL or coated ss-PTL will rapidly degrade, but the degradation rates will be different if the ss PTL substrate corrodes. Therefore, this setup can be well used for an AST in which water purity is the main stressor.

The AST setup was employed for evaluating the Nb/Ti/ss-PTL in PEMWEs with an active area of 4 cm^2. On the anode side, the following interconnecting components were used: a ss-BPP with a dense coating of Ti,[19] and a Nb/Ti/ss-PTL, and for the cathode side: an uncoated multi-layer mesh-type ss-PTL (Haver & Boecker OHG) and a ss-BPP. All stainless steel components were of 1.4404 grade. An untreated carbon paper (TGP-H-90) was placed between the cathode electrode and the ss-PTL. CCMs with an Ir-based anode, Pt-based cathode and chemically stabilized Nafion 115 membrane were used for all electrochemical tests, except for the test of Fig. 10. The loading of the catalyst is 2.5 mg cm^{-2} for iridium and 0.95 mg cm^{-2} for platinum. Polarization curves up to 2 A cm^{-2} with a scan rate of 4 mA cm^{-2} s^{-1} and electrochemical impedance spectroscopy (EIS) spectra were obtained at 0.25 and 1 A cm^{-2} and an amplitude of 50 mA and 200 mA, respectively, from 50 kHz to 100 mHz. A potentiostat/galvanostat (Zahner Elektrik IM6) with a booster (Module PP240) was used for these measurements, which were carried out at 65 °C and ambient pressure. The Nb/Ti/Ti-PTL, uncoated Ti-PTL and ss-PTL were also measured for comparison purposes. Once the polarization curves and the EIS were completed, a constant current of 2 A cm^{-2} was applied for an AST for more than 1000 h.

3. Results

3.1. Morphology of the coatings

The morphology and micro-structure of the Nb/Ti coatings were analysed by SEM. Fig. 3a presents a cross-sectional image of the

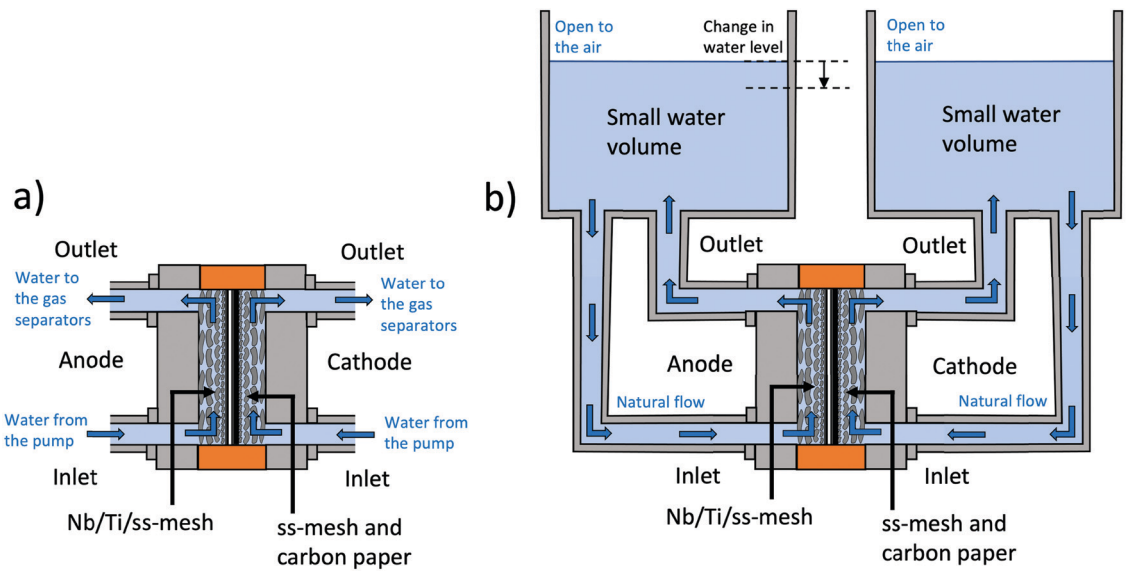

Fig. 2 (a) Conventional cell configuration for long-term tests in which DI water is flown through the anode and cathode inlets and the component corrosion products are taken away to the water loop in the BoP of the test station. (b) Cell configuration for an accelerated stress test (AST) in which the cell operates with a low volume of water under natural flow, allowing an increase in the component corrosion products and accelerating the degradation due to CCM poisoning.

Ti-PTL, showing the various layers of Ti meshes with different aperture sizes. The mesh with the lowest aperture size contacts the anode catalyst layer of the CCM, while the rest of the meshes distribute the electrical current, manage the water supply and release the formed O_2 bubbles. Ultimately, the mesh with the largest aperture size contacts the bipolar plate and acts as a flow field. The Nb/Ti coatings are applied only on the finest Ti-mesh, as shown in Fig. 3b (low magnification) and Fig. 3c (high magnification). The corresponding cross-sectional SEM images of the Nb/Ti coating deposited on the ss-PTL are displayed in Fig. 3d–f. Additional SEM images from the surface of the ss-PTL and Ti/Nb/ss-PTL are shown in Fig. S1 (ESI†).

First, the Ti layer covers almost the entire surface of the fine-mesh ss substrates, which is particularly important for protecting the PTL against the corrosive environment in the vicinity of the anode catalyst layer. Subsequent layers of Ti are porous to allow the transport of reactants and products from the water splitting process. The Ti particles of the porous layer do not form the conventional splat structure that one can observe in the dense Ti coatings[17] due to their low enthalpy during the plasma coating deposition. However, the Ti particles have a certain degree of inter-particle diffusion among each other, ensuring the mechanical stability of the coating. On top of the Ti porous layer, Nb uniformly follows the rugosity of the coating composed of Ti particles. Nb functions as an anti-passivation coating for Ti,[19] which is an alternative to costly precious metals that are normally used for extending the life-time of PEMWE cells. It is worthwhile noting that the Nb/Ti coating slightly reduces the gaps of the punched holes in the ss fine mesh, which can improve the catalyst utilization of the electrode.[9,31]

One important aspect regarding the corrosion resistance of the Nb/Ti coatings is the purity of Ti and Nb. EDS was carried out on different cross-sectional areas of the coated PTLs.

Table 1 EDS of the specific areas (MW) in Fig. 3

Area designation	O [wt%]	Si [wt%]	Ti [wt%]	Cr [wt%]	Fe [wt%]	Ni [wt%]	Nb [wt%]	Mo [wt%]
MW 1	2.36	—	0.91	—	—	—	96.73	—
MW 2	2.37	—	0.79	—	—	—	96.85	—
MW 3, 4, 5, 6	—	—	100.00	—	—	—	—	—
MW 7	3.10	—	0.35	—	—	—	96.55	—
MW 8	3.32	—	0.57	—	—	—	96.12	—
MW 9, 10	—	—	100.00	—	—	—	—	—
MW 11	0.71	0.39	0.54	16.99	68.93	10.03	—	2.40
MW 12	0.69	0.31	0.21	17.50	69.57	9.44	—	2.28

These areas are indicated as red rectangles and labelled MW in Fig. 3c and f for Nb/Ti/Ti-PTL and Nb/Ti/ss-PTL, respectively. The results of the EDS analysis are summarized in Table 1. The SEM image of Fig. 3c shows almost no colour contrast between the Ti particles (MW 3) and the Ti-mesh substrate (MW 5), suggesting that they both have the same elemental composition. The EDS results confirm that Ti-mesh substrates are pure Ti and can be considered Ti Gd1, which is the standard material for the PTL in PEMWE. Conversely, the MW 10 and 11 areas in Fig. 3f show deep contrast since these areas correspond to two very different materials, ss and Ti. The brightest material in the image corresponds to Nb. The anti-passivation layer of Nb also has a high degree of purity, and the presence of less than 1 wt% Ti is most likely attributed to the fluorescence of Ti since the measured area is quite close to the Nb/Ti interface. While EDS is not a suitable technique for measuring elements with low atomic mass, the presence of oxygen can be disregarded because during the plasma deposition process oxygen combines with the feed-stock H_2 gas to form H_2O.

3.2. Pore properties and contact resistance

The pore size distribution profiles and porosities of the Nb/Ti and Ti coatings as well as uncoated PTLs are shown in Fig. 4.

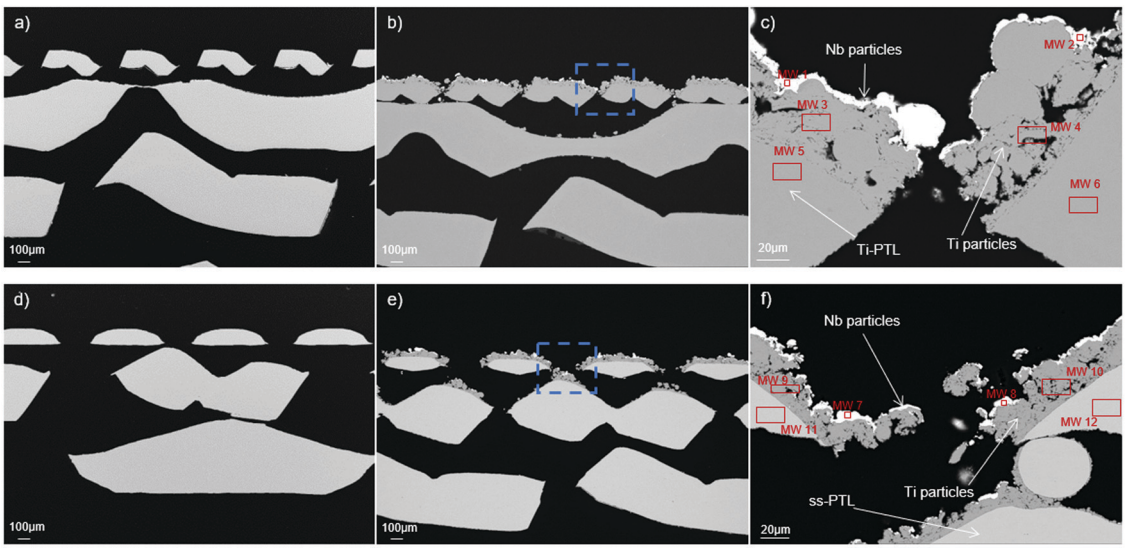

Fig. 3 Scanning electron microscopy (SEM) images of Ti-PTL (a) without and (b) with plasma-sprayed Nb/Ti coatings and ss-PTL (d) without and (e) with plasma-sprayed Nb/Ti coatings. Cutaway images of Nb/Ti on (c) Ti-PTL and (f) ss-PTL, which correspond to the blue dashed squares in (b) and (e). The solid-line squares in (c) and (f) indicate the areas where EDS was carried out, and the results are summarized in Table 1.

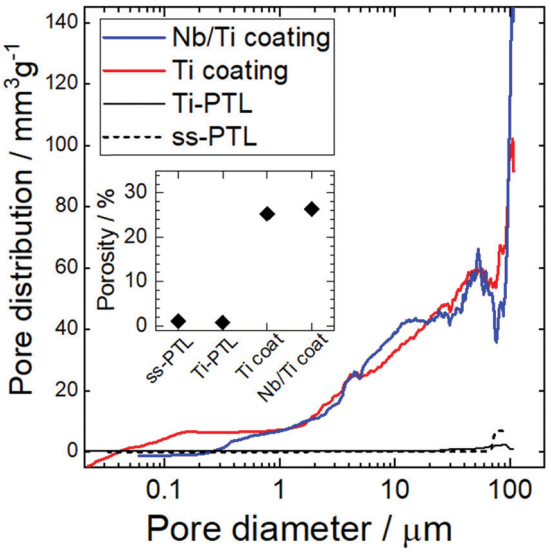

Fig. 4 Pore size distribution from mercury intrusion porosimetry (MIP) for Ti and Nb/Ti coatings on Ti-PTL or ss-mesh PTLs as well as uncoated PTLs for comparison. The inset shows the porosities of the coatings and the mesh substrates.

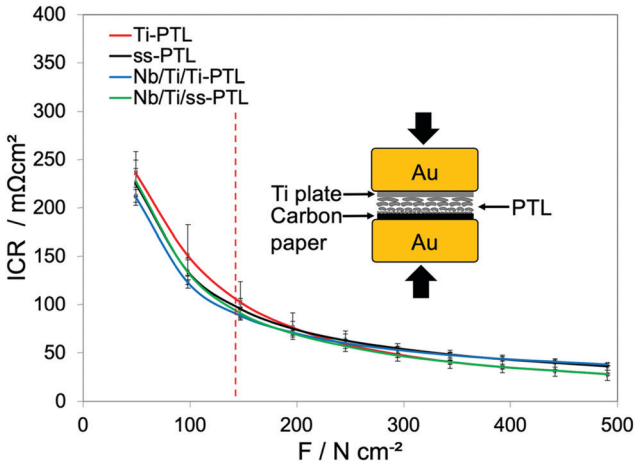

Fig. 5 Interfacial contact resistance (ICR) with respect to the compaction force of Ti-PTL, ss-PTL, Nb/Ti/Ti-PTL and Nb/Ti/ss-PTL. The inset shows a scheme of the experimental setup.

The pore distribution curve, $dV/d(\log D)$, derived by the differentiation of cumulative pore volume, is plotted per weight for each coating and uncoated Ti- and ss-PTLs for comparison. Here, variables V and D are the cumulative pore volume and the pore diameter, respectively. Both mesh PTLs are apparently dense; their pore size (or namely the gaps of the mesh) ranges above several tens of μm which is too large to be detected as pores in MIP measurements. MIP can detect the pores between a few nm and ~100 μm, and therefore, the PTL mesh is not porous and the estimated porosities are approximately 1%. In the case of the Nb/Ti and Ti coatings, the estimated porosities using eqn (1) are approximately 25% (inset of Fig. 4), and most of the pores are below several tens of μm down to 3 μm, at which diameter the distribution curve increases sharply. It should be noted here that the achievable total pore volume in MIP is limited due to the small volume of the coating compared to the dense substrate; therefore, the pore distribution profiles of the Nb/Ti and Ti coatings are nearly identical within the error considering the experimental limit. Thus, the pore size distribution of the coatings is in good agreement with the observed morphology by SEM in Fig. 3.

In addition to the optimized pore properties of Nb/Ti/ss-PTL, a good electrical connection between the plasma-sprayed coating and the catalyst layers ensures high performance due to low ICR. The ICR measurements of the Nb/Ti/ss-PTL, Nb/Ti/Ti-PTL, and uncoated PTL substrates with respect to the compaction force are presented in Fig. 5. The method for estimating the ICRs of the plasma-sprayed coatings has been previously reported,[11,19] and the experimental setup is schematized in the inset of Fig. 5. A thin sheet of carbon paper is placed between the PTLs and one of the Au-coated Cu cylinders. The ICR between the Nb/Ti coating and the anode catalyst layer can be approximated by using a carbon paper sheet instead of the Ir-based layer, as both have high in-plane electrical conductivity. Furthermore, carbon paper acts as a material that can be compressed in the applied range of compaction forces.

First, Fig. 5 reveals that all PTLs have relatively the same ICR, which is approximately 100 mΩ cm^2 at a compaction force of 150 N cm^{-2}, corresponding to the compression of the PEMWE cell during the assembly. This result is quite remarkable, although it might be characteristic of only multi-layer mesh-type PTLs. In contrast, Bernt *et al.*[32] and Kang *et al.*[33] report different resistance values between different PTLs, with and without MPL coating. For this kind of PTL, the Nb/Ti coatings have essentially no influence at all in the ICR of the PTL, and this effect should be reflected in the PEMWE tests. However, we will demonstrate in the next section that the Nb/Ti coating has a strong influence on the performance of the PEMWE in which the coating reduces ohmic losses at high current densities.

3.3. Electrochemical performance and simulation

From the ICR results with the ss-PTL and Nb/Ti/ss-PTL, which showed practically no differences in ohmic resistance, one could infer that the Nb/Ti coating will only serve to protect the ss-PTL against corrosion. Compared with the use of the uncoated Ti-PTL, any additional advantages when using the Nb/Ti/ss-PTL would be expected in the PEMWE performance, as the ohmic resistance is the same for both PTLs.

Fig. 6a shows the E_{Cell}–j characteristics of a PEMWE cell with the ss-PTL, Nb/Ti/ss-PTL, and Nb/Ti/Ti-PTL and the E_{Cell} values at a constant 2 A cm^{-2}. We observe that the use of an uncoated ss-PTL causes rapid cell depolarization, reaching up to 2.28 V at only 0.4 A cm^{-2}. The cell is only operated up to this current density, and therefore, the E_{Cell} at a constant 2 A cm^{-2} is not plotted. The PEMWE cell becomes inoperable afterwards, turning the feedstock water into a yellowish solution, similar to the colour of the electrolyte used for evaluating ss-BPPs under simulated conditions of a PEMWE cell. These results provide clear evidence for the magnitude of the challenge when using ss as a base material for the manufacture of a low-cost PTL.

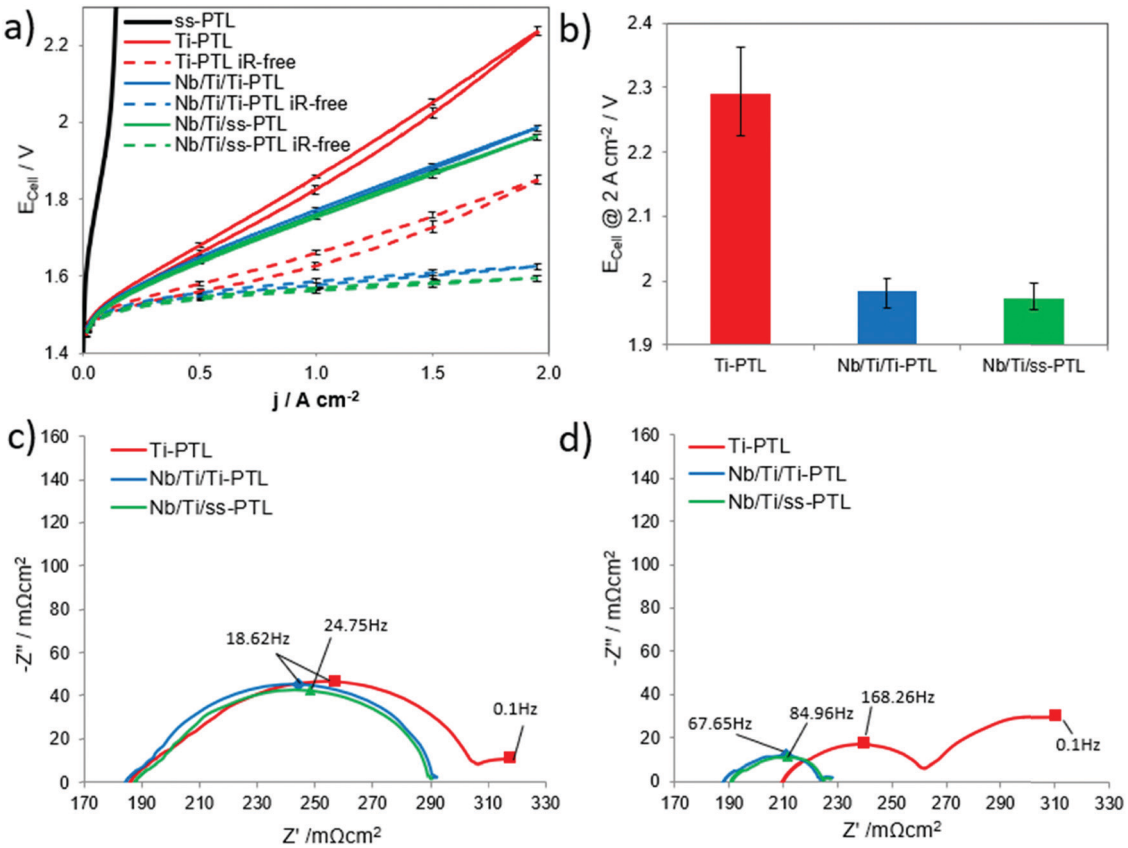

Fig. 6 (a) Polarization curves of PEMWE cells with the Ti-PTL, ss-PTL, Nb/Ti/Ti-PTL and Nb/Ti/ss-PTL. The scan rate was 4 mA cm^{-2} s^{-1}. The dashed curves show the iR-correction of the curves. (b) The cell potential values of the different PTLs at 2 A cm^{-2}. Nyquist plots at (c) 0.25 and (d) 1 A cm^{-2} from 100 mHz to 50 kHz. All measurements were carried out at 65 °C and ambient pressure.

In stark contrast, by coating the ss-PTL with Nb/Ti in PEMWE cells, it is possible to achieve performances comparable to those of commercial electrolysers, such as those from Hydrogenics,[34] Siemens[35] and Proton Onsite.[36] Clearly, the Nb/Ti coating not only protects the ss-PTL against corrosion but also has a staggering influence on the cell performance. To understand this effect, a PEMWE cell with a mesh-type Ti-PTL similar to the ss-mesh was also tested. The mesh-type Ti-PTL is the lowest cost PTL in the market, but it leads to low performances, as shown in Fig. 6a and b. Consequently, most PEMWEs use Ti felts and sinter powder plates as PTLs, although these are much more expensive than a Ti punched mesh due to the manufacturing process. First, an interesting observation is that there are large differences in the slope of the polarization curve of Ti-PTL and those of Nb/Ti/ss-PTL and Nb/Ti/Ti-PTL. At first glance, this result contradicts the observations from the ICR measurements, which show no difference in ohmic resistance among all the PTLs. Second, the polarization curve of the cell with the Ti-PTL shows a hysteric behaviour, while for the others, the forward curve overlaps with the one measured backwards. Finally, the Nb/Ti coating reduces the E_{Cell} by more than 300 mV at 2 A cm^{-2} compared with that of the uncoated Ti-PTL. This decrease in the overpotential represents an efficiency increase of approximately 12%, which has an important impact on the cost of hydrogen production. EIS will provide comprehensive explanations for all these phenomena. It is important to remark that the mesh Ti-PTL cannot be considered a baseline as the cell performance is too low compared to other well-known baselines such as the Ti felt and sintered Ti plates. However, the Ti mesh is considerably cheaper than the felt or the sintered structures and even more so is a stainless steel mesh. As a consequence, there is lot of interest from the industry to use this kind of PTL and it has potential to become the new PTL baseline in PEMWE cells. In this work we aim to use the lowest cost materials available, that is stainless steel meshes and plates to construct the PEMWE cells, and the achieved performances are comparable to other reports that use baseline sintered Ti-PTLs.[31,37] In Fig. S2 (ESI†) we show a comparison between the polarization curve of Nb/Ti/ss-PTLs in Fig. 6a and the one from a baseline Ti-PTL from GKN Sinter Metals,[38] which is commercial, and having a Pt coating applied *via* magnetron sputtering PVD.[19] The resulting curves show that the performances of the PEMWE cells with the Nb/Ti/ss-PTL and the baseline Pt/Ti-PTL (GKN Sinter Metals) are quite comparable.

The Nyquist plots of the PEMWE cell with the Ti-PTL, Nb/Ti/Ti-PTL and Nb/Ti/ss-PTL at 0.25 and 1 A cm^{-2} are shown in Fig. 6c and d, respectively. The spectra were analysed based on the equivalent circuit introduced in previous work and are shown in Fig. S3 (ESI†).[12] The ohmic resistance is given by the interception of the first semi-circle in the high-frequency

region with the *x*-axis. The resistances induced by the hydrogen evolution reaction (HER),[39] charge transfer resistance coupled with double layer effects[34] or the first charge transfer of the two-electron process of the oxygen evolution reaction (OER)[40] are represented by the high-frequency arc. The medium- and low-frequency arcs thereby describe the charge transfer of the OER rate-determining step and the mass transport losses.[41]

At 0.25 A cm^{-2}, all three cells show comparable ohmic resistance of approximately 188 ± 1 mΩ cm^2, which is in good agreement with the ICR results of Fig. 5. However, the discrepancy between the ICR and EIS could be due to the additional resistance in the catalyst layer depending on its components, such as ionomer and binder, and therefore ICR measurements cannot be directly linked to the measurements from EIS. In general, the curves for the Nb/Ti/Ti-PTL and Nb/Ti/ss-PTL are comparable to each other in their behaviour, while Ti-PTL presents a slightly larger high-frequency arc. For all samples, the second semi-circle that is associated with the OER kinetics is equivalent in size, and only for Ti-PTL there is an appearance of a small third arc with an apex at 0.1 Hz, indicating mass transport losses. In contrast, at 1 A cm^{-2}, the differences in the EIS between the cells with the coated and uncoated PTLs are very noticeable. The first most noticeable change at 1 A cm^{-2} is the increase in the ohmic resistance for Ti-PTL, while for the Nb/Ti/Ti-PTL and Nb/Ti/ss-PTL, the ohmic resistance remains almost the same at both 0.25 and 1 A cm^{-2}. Another important change in the EIS is the increase in the radius of the medium-frequency semi-circle for Ti-PTL compared to Nb/Ti/Ti-PTL and Nb/Ti/ss-PTL. Finally, the low-frequency arc of Ti-PTL increases drastically, indicating higher mass transport losses, which is in good agreement with the hysteresis shape of the polarization curve in Fig. 6a. Conversely, the mass transport effects for the coated PTLs are barely visible.[12]

The Nb/Ti coatings have a significant influence on the ohmic resistance, anode performance and mass transport behaviour during PEMWE. The ohmic resistance refers to the transitions of all cell components (PTLs, BPPs, membranes, and catalyst layers); these components should have the lowest possible resistance due to their high contact with each other. On the one hand, this contact can be worsened by the formation of non-conductive passivation layers on the Ti-PTL;[42,43] however, on the other hand, insufficient compression and thus insufficient utilization of the possible contact area can also worsen the ohmic resistance. The optimum compression of the components can be reduced by either different material expansion coefficients depending on the temperature or the conceivable formation of a gas cushion between the catalyst layer and PTL. Due to inefficient gas–water management, which can be observed in simple PTLs,[44] the produced gas accumulates at the boundary layer and reduces the contact. While no mass transport loss is observed for the coated PTLs, the Ti-PTL is the only sample that shows ohmic loss shifts to higher values; thus, mass transport limitations seem to have a decisive effect on the Ti-PTL.

Nevertheless, it should be noted that the increase in performance due to the application of the Nb/Ti coating is not only caused by the reduction in mass transport losses. The highly developed surfaces of the coated PTLs with their small porous particle layers provide a high interfacial contact area, resulting in low membrane deformation. In contrast, the region of the catalyst layer not in contact with the uncoated PTL surfaces intrudes into the large pore space, becomes degraded and thus loses conductivity. The surface of the anode at the interface between the catalyst layer and Nb/Ti/Ti-PTL or Nb/Ti/ss-PTL is highly active, whereas large areas of the interface between the catalyst layer and Ti-PTL are electrochemically inactive. This is consistent with the EIS results in Fig. 6d, which show improved kinetics of both the HER and OER, for Nb/Ti/Ti-PTL and Nb/Ti/ss-PTL. Furthermore, this finding agrees very well with the results of Schuler *et al.*,[31] who revealed that the advantage of the MPL lies in the local microscopic compression of the catalyst layer, which preserves the electrical catalyst percolation network. In addition to an increase in the catalyst utilization, this can also be understood as a reduction in membrane deformation, resulting in a significant increase in performance. Lopata *et al.*[45] came to the same conclusion and confirmed the dominance of the interface between the PTL and catalyst layer with regard to the cell performance influencing the high-frequency resistance, catalyst utilization, coverage of PTL grains due to gas bubble formation and ionomer conductivity.

PNM was employed to understand the improved mass transport phenomena in PEMWE cells with the addition of the Nb/Ti coatings. The mass transport characteristics of the coated PTLs are described by the simulated drainage curve and the capillary entry pressure of the pores. The drainage curve shown in Fig. 7 exhibits a wide range of entry capillary pressures, from approximately 780 Pa to 100 kPa. During the process of drainage, the non-wetting phase first preferentially invades pores with lower entry (threshold) capillary pressures (*i.e.*, first invades larger pores in the fine mesh substrate). Although a wide range of capillary pressures is required to fully drain the wetting phase, the wetting phase saturation dramatically decreases at the lower end of the capillary pressure curve (shown as a plateau from 1 to 0.1 in Fig. 7).

The wetting phase saturation decreases to below 10% at a capillary pressure of 3.6 kPa, indicating that most of the pore space in the coated PTL is composed of pores from the fine mesh substrate. At this capillary pressure, the larger pores (mostly from the fine mesh) are invaded by the non-wetting phase (left inset of Fig. 7), while the smaller pores (at the Nb/Ti coatings) remain uninvaded. The smaller pores become invaded after all the larger pores have been penetrated, as shown in the right inset of Fig. 7, where the small pores from the Nb/Ti coating are invaded with gas at a capillary pressure of 25 kPa. At approximately 100 kPa, the full domain of the coated PTLs becomes saturated with the non-wetting phase. To fully invade the PTL, the gas generated from the OER requires a capillary pressure build-up over an order of magnitude higher than the value to attain a 10% wetting phase saturation, which is unlikely to occur during electrolysis. Instead, the gas will break through to the larger pores in the coarser mesh by establishing a preferential transport pathway, thus leaving

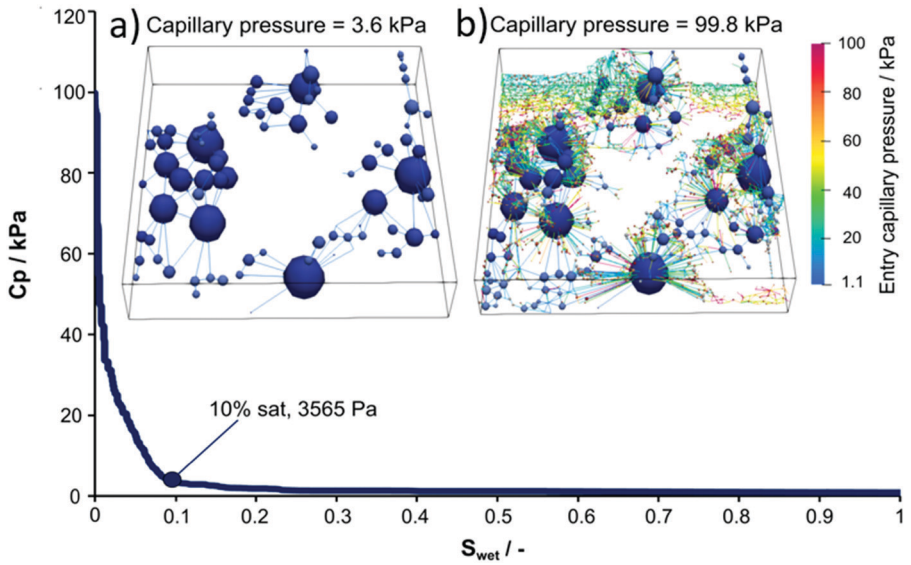

Fig. 7 Drainage characteristics generated from the pore network simulation results on the coated PTLs, (a) invaded pores and throats at capillary pressures of 3.6 kPa and (b) 99.8 kPa.

small pores in the Nb/Ti coatings uninvaded. Similar observations are reported in the previous literature.[46,47] First, Lee *et al.* revealed *via* modelling and *in operando* neutron imaging experiments that having a porosity gradient from low to high porosity facilitates mass transport during electrolysis. Moreover, they further[47] demonstrated that when a custom pore structure was applied to the PTL (*i.e.*, pores with diameters excessively larger than the average pores in the PTL), the gas saturation at the catalyst layer-PTL interface was significantly reduced and mass transport behaviour was enhanced particularly at higher current density operation. Therefore, the Nb/Ti coatings in our PTL lead to improved mass transport behaviour – the smaller pore structure (from the Nb/Ti coating) provides additional reactant transport pathways while the larger pore structure (pores from the mesh) provides effective gas removal pathways.

In contrast, during imbibition of liquid water into the PTL, the liquid water will preferentially invade pores with a higher capillary pressure (*i.e.*, smaller pores in the Nb/Ti coating). Therefore, additional transport pathways for reactant water are supplied by the small pores of the Nb/Ti coating. It is anticipated that even at high current densities, gas removal is facilitated through the large pores, and water is transported through the smaller pores in the Nb/Ti coating. In the absence of the small pores inherent in the Nb/Ti coating, reactant transport would be impeded by the gas removal process and lead to mass transport losses.

3.4. Durability under AST and post-test analysis

Fig. 6a demonstrates that the Nb/Ti coating protects the ss-PTL against corrosion for the duration of polarization. However, industry requires testing for more than 50 000 h to validate the implementation of novel components in their commercial systems.[48] Such long-term tests are impractical, and hence, the Nb/Ti/ss-PTL was evaluated under the AST described in Section 2.4. Fig. 8 shows the E_{Cell} measured at a constant 2 A cm^{-2} of PEMWE cells with the Nb/Ti/ss-PTL, Nb/Ti/Ti-PTL and Ti-PTL. The PEMWE cell with the ss-PTL is not measured since it is highly unstable and cannot withstand the applied load. Additionally, there are intermittent periods in which the cells are not operated. These intermittent interruptions are applied intentionally to resemble shut-downs and induce further degradation.

All three PEMWE cells degrade rapidly, but the cells with the Ti-PTL in particular reach E_{Cell} values close to 2.5 V, which we define as the end of test (EoT), in less than 100 h. Basically, two irreversible degradations that lead to an increase in E_{Cell} are identified in the literature: (i) an increase in ohmic resistance due to the formation of oxides at the interface of Ti-PTL[13,49] at the anode and (ii) CCM poisoning due to impurities in the water.[28,50] A third irreversible degradation mechanism is also known, which is the loss of polymeric material in the CCM, but in this case, the E_{Cell} decreases over time.[34,51] For the short time of the AST, the passivation of titanium is clearly not the dominant degradation mechanism, see Fig. S4 (ESI†), but the CCM poisoning caused by the impurities in the water that increase over time. The test with the cell with the Ti-PTL was stopped at approximately 720 h as the E_{Cell} was no longer below the EoT. A different behaviour is observed with the PEMWE cells containing the Nb/Ti/ss-PTL and Nb/Ti/Ti-PTL. The E_{Cell} values for both electrolysers have almost identical trends over time, which is a preliminary indication that the ss substrate of the Nb/Ti/ss-PTL is not corroding. Otherwise, the cell with Nb/Ti/ss-PTL should degrade faster than the cell with Nb/Ti/Ti-PTL. The ASTs for PEMWE cells with the Nb/Ti/Ti-PTL and Nb/Ti/ss-PTL were stopped at approximately 1450 h.

At the EoT, a re-assembly procedure was implemented to quantitatively determine how much the ageing of the Nb/Ti/ss-PTL contributed to the overall cell degradation and is shown in Fig. S5 (ESI†). By cleaning all metal cell components and replacing the CCM, the initial cell voltage at constant 2 A cm^{-2}

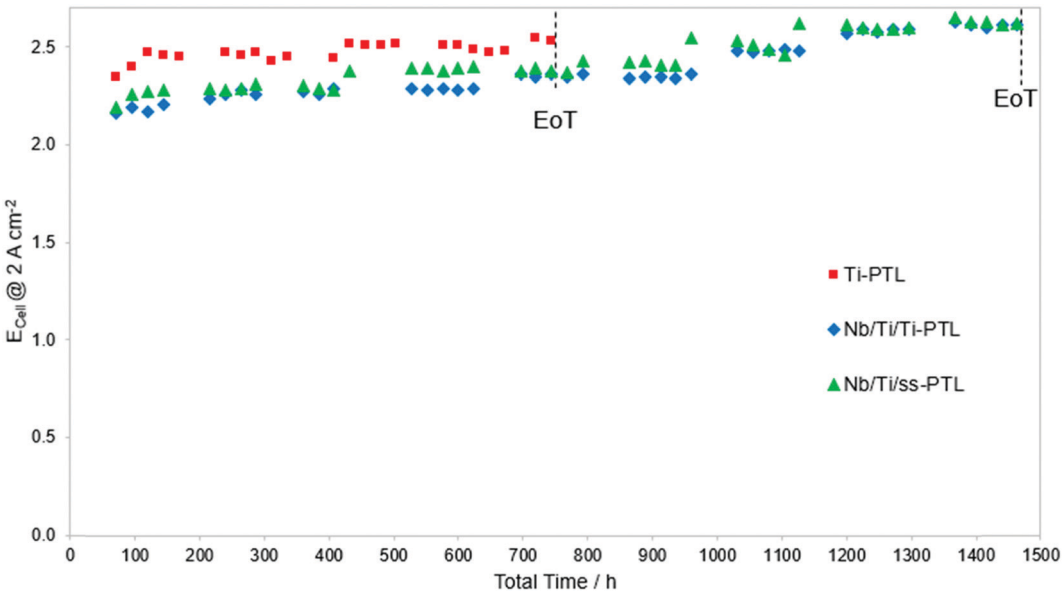

Fig. 8 Accelerated stress test (AST) of cells with the Ti-PTL, Nb/Ti/Ti-PTL and Nb/Ti/ss-PTL.

was almost completely recovered with 99%. Based on these findings, which were also observed by Sun *et al.*,[28] we conclude that the CCM is mainly responsible for the degradation of the cell. Fig. S6 (ESI†) shows the E_{Cell} *vs.* time of a PEMWE cell with Nb/Ti/ss-PTL in a conventional test station with ss pipes, pumps, gas separators, sensors, valves and other BoP components. As expected, the test in this setup does not show any increase in the E_{Cell} values due to degradation mechanisms (i) and (ii); rather, the E_{Cell} values decrease slightly over time, as is the case of an electrolyser with very stable BPPs and PTLs,[34] thus corresponding to degradation mechanism (iii).

An AST alone is still not sufficient to prove that Nb/Ti protects the ss-PTL against corrosion. If there is indeed any release of Fe^{2+} ions from the ss-PTL, it should be present in the post-tested CCM. Elemental mapping with EDS was carried out on the CCMs of PEMWE cells with Nb/Ti/ss-PTL and Nb/Ti/Ti-PTL that were subjected to the AST in Fig. 8. The results are presented in Fig. 9. The first column of images corresponds to the uncoated ss-PTL just after the first polarization curve shown in Fig. 6a. Fe (coloured in blue) is substantially present in the Ir-based anode, Pt-based cathode and Nafion membrane. In this latter component, the formed Fe crystals are most likely Fe_3O_4[15] (see Fig. S7a, ESI†). In stark contrast, the Nb/Ti/ss-PTL (second column in Fig. 9) does not show any apparent traces of Fe in the anode, cathode or membrane, which is the same as the case of the cell with Nb/Ti/Ti-PTL (third column of images in Fig. 9). This characterization of the post-tested CCMs in the PEMWE cells with the coated ss-PTL and ss-BPP for the anode and the uncoated ss-PTL and ss-BPP for the cathode clearly demonstrates that ss can be used as a base material for manufacturing the metal components of the entire electrolyser. Additionally, the SEM images of the uncoated ss-PTL and Nb/Ti/ss-PTL after the AST are shown in Fig. S8 (ESI†). The surface of the ss-PTL was clearly eroded due to the corrosion in the PEMWE cell while for the Nb/Ti/ss-PTL, no sign of degradation can be observed in either the Nb/Ti coating or the ss-PTL substrate. Lastly, X-ray photoelectron emission spectrometry (XPS) measurements, Fig. S9 (ESI†), did not reveal any Fe on the cathode of the CCM of the cell with the Nb/Ti/Ti-PTL that pass from the anode to the cathode across the PEM and inductive coupled plasma mass spectrometry (ICP-MS) of a water sample taken at the end of the test shown in Fig. 8 did not detect any increase of Fe.

3.5. Next generation PEMWE

To reduce the cost of green hydrogen further, the PEMWE cells will have to operate at much higher current densities than 2 A cm^{-2}, *e.g.* 4 A cm^{-2} as nominal load and 6 A cm^{-2} as overload,[52] while keeping efficiencies above 70%. This will only be possible if the temperature is increased to 80 °C or above and the stack uses thin membranes such as Nafion 212, and not Nafion 115, which is the state of art. Hence, one can wonder if the coated stainless-steel PEMWE components reported herein will be suitable for the next generation of PEMWE cells that will have thinner membranes than current ones and will operate up to 6 A cm^{-2} at 80 °C. Fig. 10 shows the polarization curve of a PEMWE cell with Nafion 212, Nb/Ti/ss-PTL and the other stainless steel components described in Section 2.4. As shown in the figure, the PEMWE cell can achieve an unprecedented efficiency of 77% at 4 A cm^{-2} and 80 °C. Furthermore, the slope of the polarization curve is kept straight up to 6 A cm^{-2}, in the forward and backward direction. If the curve would present hysteresis it would be an indication of mass transport losses[12] caused by Nb/Ti coating on the ss-PTL or degradation, as shown in Fig. 6a. The performance of the PEMWE cell with stainless steel components is comparable to the highest performances reported up to now by renowned R&D institutes in electrolysis.[31,37,53,54] However, thin membranes such as Nafion 212 are not yet suitable for industrial PEMWE since they degrade much faster than Nafion 115 leading to an increased H_2 crossover into the O_2 stream and

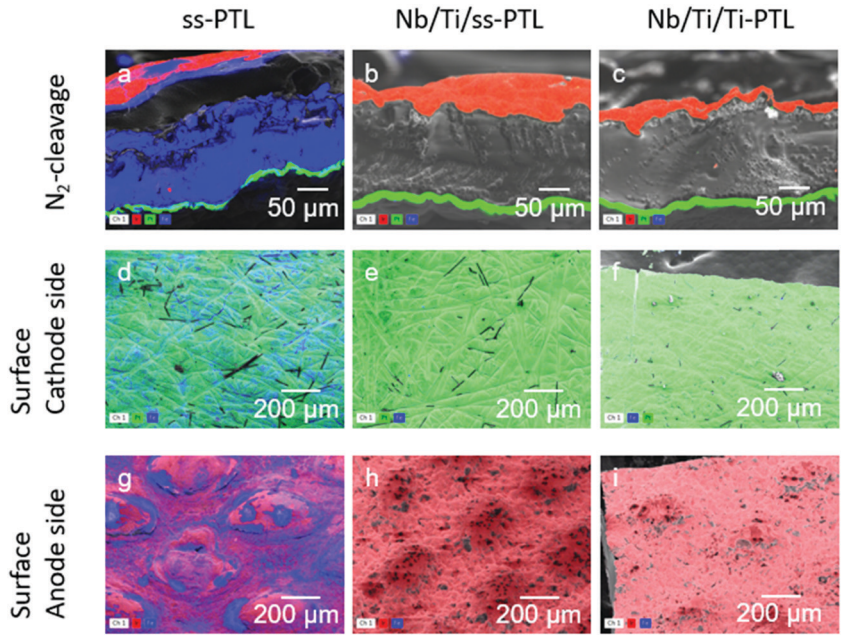

Fig. 9 EDX mapping of the (a–c) cross-section of the CCM, (d–f) cathode and (g–i) anode surfaces of the PEMWE cell with the uncoated ss-PTL, Nb/Ti/Ti-PTL, and Nb/Ti/ss-PTL.

thus compromising the safety of the electrolyser. However, it is expected that R&D institutes as well as companies like Chemours and Solvay will solve this issue in the upcoming years.

Regarding the cost/scalability of the vacuum plasma spraying technique for the deposition of Nb/Ti on the ss-PTL we have previously estimated a cost for the coating (without Nb) of about 20–100 USD m^{-2}.[17] The cost of coating production is significantly low, but it could be decrease further if the coatings are applied in a line of production, where the torch is sweeping and spraying the materials continuously on the substrate, which is either a mesh-type PTL or a flat BPP. The substrates can be produced in large area metal rolls that can be un-folded during the coating process. Industrial plasma spraying processes are scalable but one challenge may be the use of vacuum that contributes to cost that is more sensitive for the electrolysis application than for traditional uses of VPS (*e.g.* coating of turbine blades or implants). In this regard, further investigations in the future are needed to produce Nb/Ti coatings *via* atmospheric plasma spraying (APS), without affecting the structure, mechanical integrity and purity of the coatings.

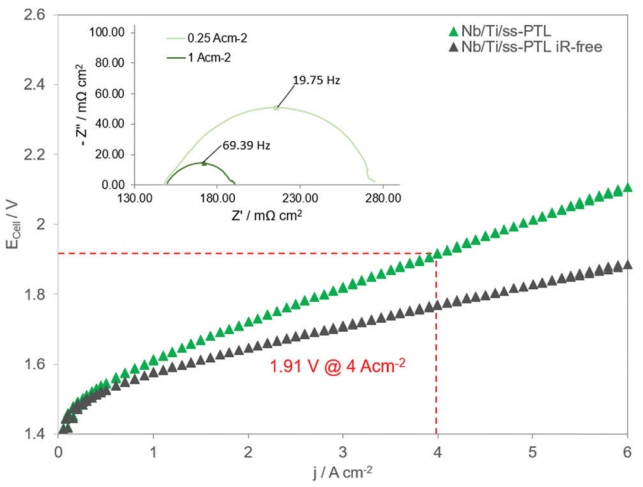

Fig. 10 Polarization curve and the iR-free curve up to 6 A cm^{-2} of a PEMWE cell with Nb/Ti/ss-PTL. The cell was operated at 80 °C and using a CCM with Nafion 212. The inset shows Nyquist plots of the cell at 0.25 and 1 A cm^{-2} from 100 mHz to 50 kHz.

4. Conclusion

There is an urgent need for reducing the cost of large PEMWE cells, and here, we have presented a solution that addresses the most expensive stack components, which are the BPPs and PTLs. Previously, we demonstrated that BPPs can be manufactured with ss,[17] but in this study, we solved a far more difficult challenge, which is the use of ss for PTLs. We developed a non-precious metal coating of Nb/Ti and applied it on the most inexpensive structure that can be used as a PTL in PEMWE, which is a ss mesh. The Nb/Ti fully protected the ss-PTL against corrosion, as the physical analyses revealed after a more than 1000 h AST for durability. Furthermore, the Nb/Ti coating on the ss-PTL reduced the cell overpotential by more than 300 mV at 2 A cm^{-2}, resulting in an efficiency increase of 12%. As the EIS measurements confirmed, these positive effects were more evident at current densities above 0.25 A cm^{-2} due to the following factors:

(i) A reduction in the ohmic resistance, which is caused by gas formation at the interface with the anode.

(ii) An improved utilization of the anode catalyst resulting in enhanced OER kinetics.

(iii) A reduction in mass transport losses.

To further understand the observed phenomena, PNM showed that the advantage of the Nb/Ti coating was explicitly due to the preferred transport of water and gas to and from the active surfaces of the anode. With the results presented herein, it can be concluded that Ti can be ruled out as a base material for the manufacture of expensive porous structures for PTLs; instead, low-cost ss meshes can be used. Moreover, ss meshes with different aperture sizes allow the use of flat plates as BPPs, which can also be manufactured in ss, without a flow field. Thus, the cost of a PEMWE cell has been reduced drastically by being almost entirely made of ss, establishing this technology as the most promising solution for the production of green hydrogen from renewable sources.

Author contributions

S. Stiber carried out the ICR and PEMWE measurements. N. Sata performed the MIP on the coatings. T. Morawietz analysed the samples by SEM. A. Fallisch carried out the micro-CT measurements. S. A. Ansar produced the Nb/Ti coatings by plasma spraying. J. K. Lee, A. Bazylak, and T. Jahnke developed the PNM. A. S. Gago led the development, tests and characterization of the PTLs. K. A. Friedrich supervised the overall work with regular discussions. All the authors contributed to writing and proofing the manuscript.

Conflicts of interest

The authors declare no competing interests.

Acknowledgements

The research leading to these results has received funding from the European Union's Horizon 2020 research and innovation programme under grant agreement No. 779478 (PRETZEL project), which is supported by FCH JU. Furthermore, funding from the European Union's Horizon 2020 research and innovation programme under grant agreement No. 862253 (PROMET-H2) was received. The authors thank Ina Plock, Günther Roth and Jörg Bürkle for performing the SEM measurements, the production of the coatings on the PTLs by VPS and the technical support, respectively. The authors also acknowledge the support from G. Moutinho and A. Martinez Séptimo in carrying out the PEMWE measurements as part of their master theses. The authors acknowledge Lukas Mues and Nina Bengen for ICP-MS measurements as well as Dr. Indro Biswas, Prof. Thomas Chassé and Dustin O'Neill Quinones for providing XPS analysis. Finally, the authors thank Vincent Wilke for supporting the preparation of the revised version since the first author Svenja Stiber was in maternity leave.

References

1 A. Buttler and H. Spliethoff, Current status of water electrolysis for energy storage, grid balancing and sector coupling via power-to-gas and power-to-liquids: A review, *Renewable Sustainable Energy Rev.*, 2018, **82**, 2440–2454, DOI: 10.1016/j.rser.2017.09.003.
2 J. Eichman, K. Harrison and M. Peters, *Novel Electrolyzer Applications: Providing More Than Just Hydrogen*, National Renewable Energy Laboratory, 2014.
3 M. Carmo, D. L. Fritz, J. Mergel and D. Stolten, A comprehensive review on PEM water electrolysis, *Int. J. Hydrogen Energy*, 2013, **38**, 4901–4934, DOI: 10.1016/j.ijhydene.2013.01.151.
4 FCH-JU, Addendum to the Multi-Annual Work Plan 2014-2020, Fuel Cells and Hydrogen 2 Joint Undertaking (2018).
5 J. O. Majasan, F. Iacoviello, P. R. Shearing and D. J. L. Brett, Effect of Microstructure of Porous Transport Layer on Performance in Polymer Electrolyte Membrane Water Electrolyser, *Energy Procedia*, 2018, **151**, 111–119.
6 K. Bromberger, G. Jagdishkumar, T. Lickert, A. Fallisch and T. Smolinka, Hydraulic ex situ through-plane characterization of porous transport layers in PEM water electrolysis cells, *Int. J. Hydrogen Energy*, 2018, **43**, 2556–2569.
7 T. Lickert, M. L. Kiermaier, K. Bromberger, G. Jagdishkumar, S. Metz, A. Fallisch and T. Smolinka, On the influence of the anodic porous transport layer on PEM electrolysis performance at high current densities, *Int. J. Hydrogen Energy*, 2020, **45**, 6047–6058.
8 S. Park, J.-W. Lee and B. N. Popov, A review of gas diffusion layer in PEM fuel cells: Materials and designs, *Int. J. Hydrogen Energy*, 2012, **37**, 5850–5865.
9 Z. Kang, J. Mo, G. Yang, S. T. Retterer, D. A. Cullen, T. J. Toops, J. B. Green Jr, M. M. Mench and F.-Y. Zhang, Investigation of thin/well-tunable liquid/gas diffusion layers exhibiting superior multifunctional performance in low-temperature electrolytic water splitting, *Energy Environ. Sci.*, 2017, **10**, 166–175.
10 T. Schuler, R. De Bruycker, T. J. Schmidt and F. N. Büchi, Polymer Electrolyte Water Electrolysis: Correlating Porous Transport Layer Structural Properties and Performance: Part I. Tomographic Analysis of Morphology and Topology, *J. Electrochem. Soc.*, 2019, **166**(4), F270–F281.
11 P. Lettenmeier, S. Kolb, F. Burggraf, A. S. Gago and K. A. Friedrich, Towards developing a backing layer for proton exchange membrane electrolyzers, *J. Power Sources*, 2016, **311**, 153–158.
12 P. Lettenmeier, S. Kolb, N. Sata, A. Fallisch, L. Zielke, S. Thiele, A. S. Gago and K. A. Friedrich, Comprehensive investigation of novel pore-graded gas diffusion layers for high-performance and cost-effective proton exchange membrane electrolyzers, *Energy Environ. Sci.*, 2017, **10**, 2521–2533.
13 C. Rakousky, U. Reimer, K. Wippermann, M. Carmo, W. Lueke and D. Stolten, An analysis of degradation phenomena in polymer electrolyte membrane water electrolysis, *J. Power Sources*, 2016, **326**, 120–128.
14 C. Liu, M. Shviro, A. S. Gago, S. F. Zaccarine, G. Bender, P. Gazdzicki, T. Morawietz, I. Biswas, M. Rasinski, A. Everwand, R. Schierholz, J. Pfeilsticker, M. Müller, P. P. Lopes, R.-A. Eichel, B. Pivovar, S. Pylypenko,

K. A. Friedrich, W. Lehnert and M. Carmo, Exploring the Interface of Skin-Layered Titanium Fibers for Electrochemical Water Splitting, *Adv. Energy Mater.*, 2021, **11**, 2002926.

15 J. Mo, S. M. Steen, F. Y. Zhang, T. J. Toops, M. P. Brady and J. B. Green, Electrochemical investigation of stainless steel corrosion in a proton exchange membrane electrolyzer cell, *Int. J. Hydrogen Energy*, 2015, **40**, 12506–12511.

16 J. Mo, S. Steen, Z. Kang, G. Yang, D. A. Taylor, Y. Li, T. J. Toops, M. P. Brady, S. T. Retterer, D. A. Cullen, J. B. Green and F. Y. Zhang, Study on corrosion migrations within catalyst-coated membranes of proton exchange membrane electrolyzer cells, *Int. J. Hydrogen Energy*, 2017, **42**, 27343–27349.

17 A. S. Gago, S. A. Ansar, B. Saruhan, U. Schulz, P. Lettenmeier, N. A. Cañas, P. Gazdzicki, T. Morawietz, R. Hiesgen, J. Arnold and K. A. Friedrich, Protective coatings on stainless steel bipolar plates for proton exchange membrane (PEM) electrolysers, *J. Power Sources*, 2016, **307**, 815–825.

18 P. Lettenmeier, R. Wang, R. Abouatallah, F. Burggraf, A. S. Gago and K. A. Friedrich, Coated Stainless Steel Bipolar Plates for Proton Exchange Membrane Electrolyzers, *J. Electrochem. Soc.*, 2016, **163**, F3119–F3124.

19 P. Lettenmeier, R. Wang, R. Abouatallah, B. Saruhan, O. Freitag, P. Gazdzicki, T. Morawietz, R. Hiesgen, A. S. Gago and K. A. Friedrich, Low-Cost and Durable Bipolar Plates for Proton Exchange Membrane Electrolyzers, *Sci. Rep.*, 2017, **7**, 44035.

20 N. Rojas, M. Sánchez-Molina, G. Sevilla, E. Amores, E. Almandoz, J. Esparza, M. R. Cruz Vivas and C. Colominas, Coated stainless steels evaluation for bipolar plates in PEM water electrolysis conditions, *Int. J. Hydrogen Energy*, 2021, **46**(51), 25929–25943.

21 P. Shirvanian and F. Van Bekel, Novel components in Proton Exchange Membrane (PEM) Water Electrolyzers (PEMWE): Status, challenges and future needs. A mini review, *Electrochem. Commun.*, 2020, **114**, 106704.

22 L. Bertuccioli, A. Chan, D. Hart, F. Lehner, B. Madden and E. Standen, *Development of Water Electrolysis in the European Union*, Fuel Cells and Hydrogen Joint Undertaking, 2014.

23 K. Ayers, N. Danilovic, R. Ouimet, M. Carmo, B. Pivovar and M. Bornstein, Perspectives on Low-Temperature Electrolysis and Potential for Renewable Hydrogen at Scale, *Annu. Rev. Chem. Biomol. Eng.*, 2019, **10**, 219–239.

24 N. F. Daudt, F. J. Hackemüller and M. Bram, Powder metallurgical production of 316L stainless steel/niobium composites for Proton Exchange membrane electrolysis cells, *Powder Metall.*, 2019, **62**, 176–185, DOI: 10.1080/00325899.2019.1607461.

25 GeoDict, www.geodict.com. 11/30/2018.

26 J. Gostick, Versatile and efficient pore network extraction method using marker-based watershed segmentation, *Phys. Rev. E*, 2017, **96**(2), 023307.

27 J. Gostick, M. Aghighi, J. Hinebaugh, T. Tranter, M. Hoeh, H. Day, B. Spellacy, M. Sharqawy, A. Bazylak, A. Burns, W. Lehnert and A. Putz, OpenPNM: A Pore Network Modeling Package, *Comput. Sci. Eng.*, 2016, **18**(4), 60–74.

28 S. Sun, Z. Shao, H. Yu, G. Li and B. Yi, Investigations on degradation of the long-term proton exchange membrane water electrolysis stack, *J. Power Sources*, 2014, **267**, 515–520, DOI: 10.1016/j.jpowsour.2014.05.117.

29 Q. Feng, X. Z. Yuan, G. Liu, B. Wei, Z. Zhang, H. Li and H. Wang, A review of proton exchange membrane water electrolysis on degradation mechanisms and mitigation strategies, *J. Power Sources*, 2017, **366**, 33–55, DOI: 10.1016/j.jpowsour.2017.09.006.

30 P. Aßmann, A. S. Gago, P. Gazdzicki, K. A. Friedrich and M. Wark, Toward developing accelerated stress tests for proton exchange membrane electrolyzers, *Curr. Opin. Electrochem.*, 2020, **21**, 225–233, DOI: 10.1016/j.coelec.2020.02.024.

31 T. Schuler, J. M. Ciccone, B. Krentscher, F. Marone, C. Peter, T. J. Schmidt and F. N. Büchi, Hierarchically Structured Porous Transport Layers for Polymer Electrolyte Water Electrolysis, *Adv. Energy Mater.*, 2020, **10**, 1903216, DOI: 10.1002/aenm.201903216.

32 M. Bernt and H. A. Gasteiger, Influence of Ionomer Content in IrO2/TiO2 Electrodes on PEM Water Electrolyzer Performance, *J. Electrochem. Soc.*, 2016, **163**, F3179–F3189, DOI: 10.1149/2.0231611jes.

33 Z. Kang, S. M. Alia, M. Carmo and G. Bender, In-situ and in-operando analysis of voltage losses using sense wires for proton exchange membrane water electrolyzers, *J. Power Sources*, 2021, **481**, 229012, DOI: 10.1016/j.jpowsour.2020.229012.

34 P. Lettenmeier, R. Wang, R. Abouatallah, S. Helmly, T. Morawietz, R. Hiesgen, S. Kolb, F. Burggraf, J. Kallo, A. S. Gago and K. A. Friedrich, Durable Membrane Electrode Assemblies for Proton Exchange Membrane Electrolyzer Systems Operating at High Current Densities, *Electrochim. Acta*, 2016, **210**, 502–511, DOI: 10.1016/j.electacta.2016.04.164.

35 F. J. Hackemüller, E. Borgardt, O. Panchenko, M. Müller and M. Bram, Manufacturing of Large-Scale Titanium-Based Porous Transport Layers for Polymer Electrolyte Membrane Electrolysis by Tape Casting, *Adv. Eng. Mater.*, 2019, **21**, 1801201, DOI: 10.1002/adem.201801201.

36 K. E. Ayers, J. N. Renner, N. Danilovic, J. X. Wang, Y. Zhang, R. Maric and H. Yu, Pathways to ultra-low platinum group metal catalyst loading in proton exchange membrane electrolyzers, *Catal. Today*, 2016, **262**, 121–132, DOI: 10.1016/j.cattod.2015.10.019.

37 M. Bernt, J. Schröter, M. Möckl and H. A. Gasteiger, Analysis of Gas Permeation Phenomena in a PEM Water Electrolyzer Operated at High Pressure and High Current Density, *J. Electrochem. Soc.*, 2020, **167**, 124502, DOI: 10.1149/1945-7111/ABAA68.

38 S. Stiber, H. Balzer, A. Wierhake, F. J. Wirkert, J. Roth, U. Rost, M. Brodmann, J. K. Lee, A. Bazylak, W. Waiblinger, A. S. Gago and K. A. Friedrich, Porous Transport Layers for Proton Exchange Membrane Electrolysis under Extreme Conditions of Current Density, Temperature and Pressure, *Adv. Energy Mater.*, 2021, **11**, 2100630, DOI: 10.1002/aenm.202100630.

39 S. Siracusano, S. Trocino, N. Briguglio, V. Baglio and A. S. Aricó, Electrochemical Impedance Spectroscopy as a

Diagnostic Tool in Polymer Electrolyte Membrane Electrolysis, *Materials*, 2018, **11**, 1368.

40 C. Rozain, E. Mayousse, N. Guilleta and P. Millet, Influence of iridium oxide loadings on the performance of PEM water electrolysis cells: Part II – Advanced oxygen electrodes, *Appl. Catal., B*, 2016, **182**, 123–131.

41 M. Eikerling and A. A. Kornyshev, Electrochemical impedance of the cathode catalyst layer in polymer electrolyte fuel cells, *J. Electroanal. Chem.*, 1999, **475**, 107–123.

42 M. Metikos-Hukovic and M. Ceraj-Ceric, Anodic oxidation of Titanium: Mechanism of non-stoichiometric oxide formation, *Surf. Technol.*, 1985, **24**, 273–283, DOI: 10.1016/0376-4583(85)90077-9.

43 P. Millet, N. Mbemba, S. A. Grigoriev, V. N. Fateev, A. Aukauloo and C. Etiévant, Electrochemical performance of PEM water electrolysis cells and perspectives, *Int. J. Hydrogen Energy*, 2011, **36**, 4134–4142.

44 J. Van der Merwe, K. Uren, G. Van Schoor and D. Bessarabov, Characterization tools development for PEM electrolysers, *Int. J. Hydrogen Energy*, 2014, **39**(26), 14212–14221.

45 J. Lopata, Z. Kang, J. Young, G. Bender, J. W. Weidner and S. Shimpalee, Effects of the Transport/Catalyst Layer Interface and Catalyst Loading on Mass and Charge Transport Phenomena in Polymer Electrolyte Membrane Water Electrolysis Devices, *J. Electrochem. Soc.*, 2020, **167**, 064507, DOI: 10.1149/1945-7111/ab7f87.

46 J. K. Lee, C. H. Lee, K. F. Fahy, P. J. Kim, J. M. LaManna, E. Baltic, D. L. Jacobson, D. S. Hussey, S. Stiber, A. S. Gago, K. A. Friedrich and A. Bazylak, Spatially Graded Porous Transport Layers for Gas Evolving Electrochemical Energy Conversion: High Performance Polymer Electrolyte Membrane Electrolyzers, *Energy Convers. Manage.*, 2020, **226**, 113545.

47 J. K. Lee, C. H. Lee, K. F. Fahy, P. J. Kim, K. Krause, J. M. LaManna, E. Baltic, D. L. Jacobson, D. S. Hussey and A. Bazylak, Accelerating bubble detachment in porous transport layers with patterned through pores, *ACS Appl. Energy Mater.*, 2020, **3**, 9676–9684.

48 C. Chardonnet, L. De Vos, F. Genoese, G. Roig, F. Bart, J.-C. Lanoix, T. Ha and B. Van Genabet Study on early business cases for H2 in energy storage and more broadly power to H2 applications, (2017), https://www.fch.europa.eu/sites/default/files/P2H_Full_Study_FCHJU.pdf, 02/19/2020.

49 C. Liu, M. Carmo, G. Bender, A. Everwand, T. Lickert, J. L. Young, T. Smolinka, D. Stolten and W. Lehnert, Performance enhancement of PEM electrolyzers through iridium-coated titanium porous transport layers, *Electrochem. Commun.*, 2018, **97**, 96–99, DOI: 10.1016/j.elecom.2018.10.021.

50 X. Wang, L. Zhang, G. Li, G. Zhang, Z.-G. Shao and B. Yi, The influence of Ferric ion contamination on the solid polymer electrolyte water electrolysis performance, *Electrochim. Acta*, 2015, **158**, 253–257.

51 S. Siracusano, N. Hodnik, P. Jovanovic, F. Ruiz-Zepeda, M. Šala, V. Baglio and A. S. Aricò, New insights into the stability of a high performance nanostructured catalyst for sustainable water electrolysis, *Nano Energy*, 2017, **40**, 618–632, DOI: 10.1016/j.nanoen.2017.09.014.

52 PRETZEL – Novel modular stack design for high pressure PEM water electrolyzer technology with wide operation range and reduced cost. http://pretzel-electrolyzer.eu, 12/11/2020 07:01.

53 F. Scheepers, M. Stähler, A. Stähler, E. Rauls, M. Müller, M. Carmo and W. Lehnert, Improving the Efficiency of PEM Electrolyzers through Membrane-Specific Pressure Optimization, *Energies*, 2020, **13**, 612, DOI: 10.3390/en13030612.

54 S. Siracusano, C. Oldani, M. A. Navarra, S. Tonella, L. Mazzapioda, N. Briguglio and A. S. Aricò, Chemically stabilised extruded and recast short side chain Aquivion proton exchange membranes for high current density operation in water electrolysis, *J. Membr. Sci.*, 2020, **578**, 136–148, DOI: 10.1016/j.memsci.2019.02.021.

